Applied Materials Today 18 (2020) 100500

Contents lists available at ScienceDirect

Applied Materials Today

journal homepage: www.elsevier.com/locate/apmt

Genetically engineered elastin-like recombinamers with sequence-based molecular stabilization as advanced bioinks for 3D bioprinting

Soraya Salinas-Fernández, Mercedes Santos, Matilde Alonso, Luis Quintanilla, Jose Carlos Rodríguez-Cabello*

BIOFORGE (Group for Advanced Materials and Nanobiotechnology), CIBER-BBN, University of Valladolid. 47011, Valladolid, Spain

ARTICLE INFO

Article history:
Received 23 July 2019
Received in revised form 26 October 2019
Accepted 4 November 2019

Keywords:
3d bioprinting
Novel bioinks
Advanced materials
Tissue engineering
Elastin like recombinamers

ABSTRACT

The versatility of 3D bioprinting techniques has demonstrated great potential for the development of artificial engineered tissues that more closely resemble native tissues. Despite this, challenges remain as regards the search for new bioinks that embrace all the complex parameters that this technique demands. In an attempt to develop such an advanced material, a novel smart material based on elastin-like recombinamers (ELRs) has been developed by molecularly programming its sequence to exhibit a sequential three-stage gelation process, thus providing printing attributes.

The thermoresponsive behavior of the ELR is exploited for the deposition of well-controlled fibres on a platform heated to 37 °C, and its recombinant nature ensures batch-to-batch reproducibility and its applicability to a desired target tissue by the introduction of selected bioactive amino-acid sequences into its molecular chain.

The biocompatible nature of the ELR enables the printing of loaded cells while providing a protective environment as part of the printing process. Thus, HFF-1 cells were found to be able to proliferate within the printed structures upon culture, displaying their natural morphology.

The results of this work highlight the applicability and novelty of the bioprinting of biomimetic ELR-based structures for advanced applications.

1. Introduction

Determination of the most suitable bioink is fundamental for the successful production of printed tissue-mimetic structures. However, the strict requirements of the 3D printing technique itself in terms of printability [1], biological parameters [2] and mechanical and structural properties [3] are such that currently used bioinks are limited by their properties, thus restricting the potential applications of this technique [4].

Structural and mechanical properties are the main disadvantages found in naturally derived materials developed as bioinks such as alginate, gelatin, collagen, RGD peptides, silk fibroin or fibrin, which otherwise usually provide an environment comparable to that of the extracellular matrix [5]. In contrast, synthetic materials such as poly(co-glycolic lactic acid) (PLGA) [6], pluronic acid [7,8], poly(ethylene glycol) (PEG) [9], poly(L-lactic acid) (PLA) and poly(ε-caprolactone) (PCL), which normally exhibit better printability, are unable to provide a proper cell proliferative environment. Given that the majority of used inks have not been specifically designed for 3D bioprinting applications, a genuine breakthrough in the development of new inks would depend on the non-trivial rationality of a new natural biological material that, in turn, can be molecularly designed from scratch in order to comply with the wide variety of parameters that determine its structural, mechanical and biological behavior.

If developed for use as bioinks, protein-based materials could demonstrate such exceptional features since proteins already play an important role in a wide variety of tissue specific functions, which endow them with a high complexity.

One example of this proteinaceous materials are the Elastin Like Recombinamers (ELRs) whose aminoacidic structure is inspired from the arrangement of the highly repetitive and well-conserved domains of the mammalian tropoelastin [10,11]. The hydrophobic VPGXG pentapeptide is one of the most well-known repetitive sequence within the ELR family, where X can be selected to modulate the final polymeric properties [12,13].

ELRs are produced via recombinant DNA technologies, which allow designing the sequences to show specific properties required

* Corresponding author.
E-mail address: roca@bioforge.uva.es (J.C. Rodríguez-Cabello).

https://doi.org/10.1016/j.apmt.2019.100500

for a certain application, through an extremely precise control over the amino acid composition.

The fact that ELRs are inspired into the elastin sequence, makes them acquire several of its interesting properties and for this reason, ELRs have emerged as useful candidates for several biomedical applications [14–16] showing an excellent biocompatibility [17], biodegradability and adjustable mechanical properties. Perhaps more interestingly for 3D bioprinting applications, is that they exhibit a smart behavior of thermo-responsiveness defined by the so-called Inverse Temperature Transition (ITT). So, in aqueous solution and below the transition temperature (Tt) of the recombinamer, the polymer chains remain soluble in a random coil conformed by hydrophobic hydration. If temperature rises above the Tt of the polymer, a hydrophobic folding is induced [18], leading to hydrogel formation when high concentration is used.

This reversible phase transition can be seized for the ELRs deposition into 3D architectural matrixes.

The difficulty when designing the molecular structure that an ELR must exhibit in order to behave as an ink lies in inducing the properties of printability and stability during its self-assembly into a supramolecular hydrogel. As such, the hypothesis of our research was to obtain a bioprintable ELR hydrogel that enables the creation of advanced printed scaffolds which show structural stability over time. To that end, a complex sol-gel transition of the ELR was induced by way of three consecutive gelation stages with different kinetics, as follows:

(1) A primary thermally induced fast gelation based on hydrophobic interactions to ensure quick responsiveness. This is achieved by engineering the backbone of the ELR using a hydrogel comprising a previously reported amphiphilic tetrablock recombinamer known as EI [19].
(2) A subsequent second stabilization that provides structural stability during printing due to the incorporation of a leucine zipper domain taken from the dimerization domain of the hepatic leukemia factor (HLF) [20]. This leucine zipper domain (Z) was selected due to its ability to form amphiphilic α-helical structures whose hydrophobic interactions drives them to associate into a coiled-coil model [21]. The Z-moiety is intended to be placed at the beginning of the gene sequence to prevent it from being hidden during folding of the structure, thus enabling the sequence to also dimerize with surrounding chains, thereby hindering the molecular structures and avoiding slippages.
(3) A third programmed stabilization intended to induce a progressive consolidation of the printed structures by inclusion of a silk-like sequence in combination with the EI tetrablock, thus combining elastin and silk properties [22]. A consensus *Bombyx mori* fibroin peptide $(GAGAGS)_5$ will be used for this purpose. The tendency of this peptide to associate via beta-sheets will result in a tightening of the structure over time.
(4) Finally, a terminal bioactive block $([VPGIG]_5$-$AVTGRGDSPASS)_6)$ containing the well-known integrin-dependent cell-adhesion RGD tripeptide is placed at the C-terminus of the final polypeptide chain to improve cell-recombinamer interactions. This approach intended to overcome the disadvantages of synthetic inks with respect to lack of cell adhesion and proliferation [23,24].

A scheme of the gelation contribution to the whole molecule, provided by each peptide block, can be seen in Fig. 1:

The sequentially gelation mechanism of the hydrogel described above will yield to an extrudable ink with high printability avoiding the need for any exogenous crosslinking mechanism.

In this study, for the first time, we demonstrate the potential use of the ELRs as materials to construct resolutive cell-laden tissue matrixes which, in turn, provide an extracellular matrix-like environment sufficient to induce cell proliferation and differentiation.

The designed and bioproduced novel ELR was evaluated for its printability, rheological and mechanical properties. Also cell viability and morphology were measured as a result of the printing process.

2. Materials and methods

2.1. Synthesis and characterization of ZS-EI-ELR and control recombinamers

The new ELR was designed and synthesised using a "recursive directional ligation" (RDL) strategy previously used and fully described [25,26].

After modified *Escherichia coli* cultivation into a bioreactor, ultrasonic disruption of the bacterial membrane was performed to extract the ELR contained within the bacteria once the stationary phase of the bacterial culture had been achieved. Several temperature-dependent and reversible precipitation cycles were performed to purify the expressed polymer [25], followed by dialysis against deionized water and freeze-drying.

The purity and molecular weight of the recombinamer were assessed by sodium dodecyl sulfate polyacrylamide gel electrophoresis (SDS-PAGE, Figure S1, supplementary material), amino-acid composition analysis (Table S1), mass spectrometry (MALDI-TOF, Figure S2), proton nuclear magnetic resonance analysis (^{1}H NMR, Figure S3) and differential scanning calorimetry (DSC) (Figure S4).

The rest of the recombinamers used in this work were previously synthesized and characterized in our research group as previously reported: EI-ELR [27]; Z-EI-ELR [28] and S-EI-ELR [29]. A simplification of their block composition and their precise aminoacidic chain are specified into Fig. 2 and Table 1.

2.2. Printing setup

All printings were performed using a REGEMAT 3D customized printer. A coupled temperature-controlled cartridge enabled control of the reservoir temperature (Figure S5), whereas the heated bed allowed the scaffold deposition temperature to be maintained. The printing parameters were optimized and the printing process set to use 0.25 diameter blunt needles at a 1 mm/s cartridge velocity and 0.06 mm^3.s flow.

2.3. Ink printability characterization

Semi-quantification of the printability was carried out as previously reported by Liliang, O., et al. [30], who established a Printability parameter (Pr) to measure the similarity of squared-shaped printings with respect to the designed ones. The mathematical model assumes that the parameter circularity (C) value is the highest in case of circles, showing a value of 1.

$$C = \frac{4\pi A}{L^2} \tag{1}$$

For squared-shapes, instead of circles, the circularity would be $\pi / 4$, and the parameter *Pr* can be defined as:

$$\boldsymbol{Pr} = \frac{\boldsymbol{\pi}}{4} \cdot \frac{1}{\boldsymbol{C}} = \frac{\boldsymbol{L}^2}{16\boldsymbol{A}} \tag{2}$$

According to Eq. (2), the *Pr* parameter will acquire a value of 1 for an ideal printability condition, where the interconnected pores would form a perfect square. The lower the calculated *Pr* value is, the least capacity of the ink to resemble its designed structure can be found.

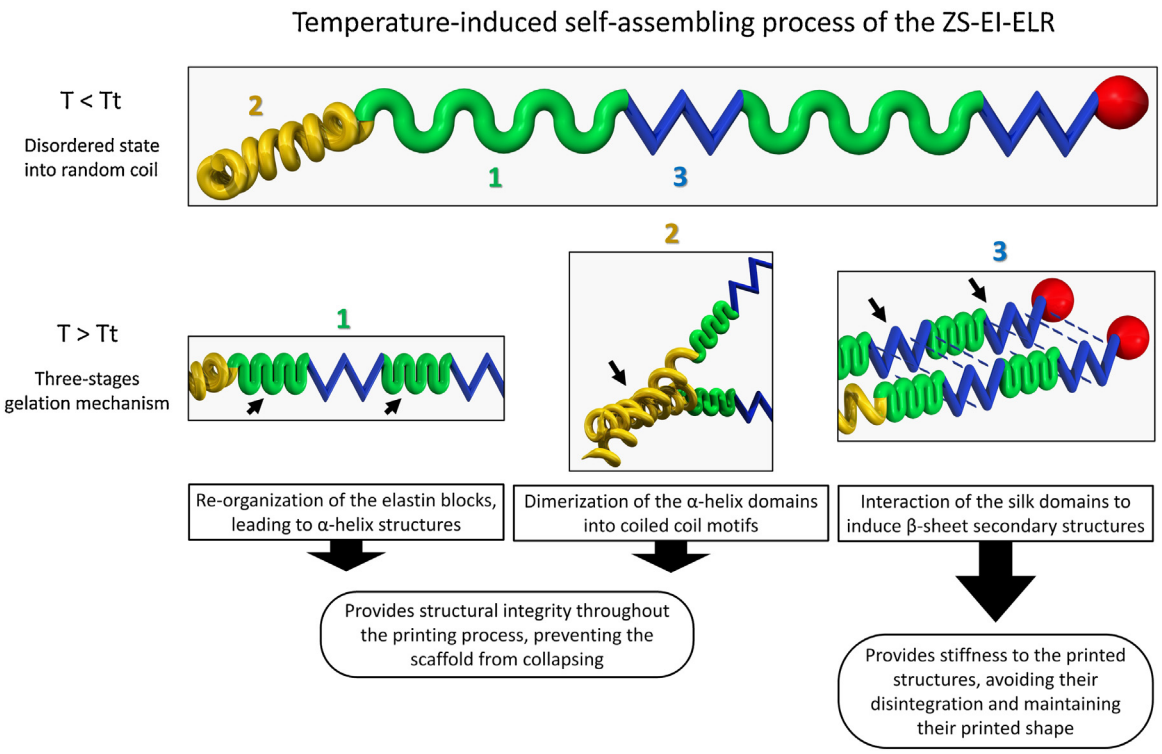

Fig. 1. Graphical scheme of the peptide blocks that constitute the novel designed ELR ink and its block molecular assembling leading to stabilisation.

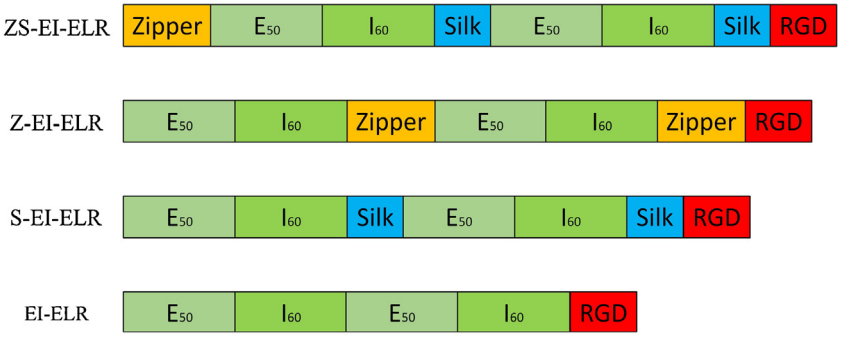

Fig. 2. Graphical scheme of the composition of the used recombinamers.

Table 1
Amino acid sequences of the ZS-EI-ELR and control recombinamers.

Recombinamer abbreviation	Amino acid sequence
ZS-EI-ELR	MESLLP-{[VGGGGGKENQIAIRASFLEKENSALRQEVADLRKELGKCKNILAKYEAGGGGG] ([(VPGVG)$_2$ - (VPGEG) - (VPGVG)$_2$]$_{10}$[VGIPG]$_{60}$)-[V(GAGAGS)5 G]$_2$}$_2$-([VPGIG]$_5$AVTGRGDSPASS)$_6$V
Z-EI-ELR	MESLLP-{[VPGVG)$_2$-(VPGEG)-(VPGVG)$_2$]$_{10}$[VGIPG]$_{60}$-[VGGGGGKENQIAIRASFLEKENSALRQEVADLRKELGKCKNILAKYEAGGGGG]}$_2$-([VPGIG]$_5$AVTGRGDSPASS)$_6$-V
S-EI-ELR	MESLLP-{([(VPGVG)$_2$-(VPGEG)-(VPGVG)$_2$]$_{10}$[VGIPG]$_{60}$)-[V(GAGAGS)$_5$G]$_2$}$_2$-([VPGIG]$_5$AVTGRGDSPASS)$_6$-V
EI-ELR	MESLLP-{[VPGVG)$_2$-(VPGEG)-(VPGVG)$_2$]$_{10}$[VGIPG]$_{60}$}$_2$-([VPGIG]$_5$AVTGRGDSPASS)$_6$-V

To that end, square grids were designed using the REGEMAT 3D specific software. These grids measured 10 × 10 mm, with a height of 1.30 mm and 1.5 mm pores at 90° angles.

The recombinamers S-EI-ELR and ZS-EI-ELR were subjected to a previously reported pre-annealing treatment in solution, by incubation at 37 °C during 24 h [31] to ensure an equal and ordered state of the β-sheet structures provided by the silk motifs for each recombinamer batch. After their pre-annealing, they were again lyophilized and stored.

For the printability characterization, lyophilized recombinamers Z-EI-ELR, S-EI-ELR and ZS-EI-ELR were dissolved 12 h before the experiments using PBS as solvent to ensure their complete dissolution, and were printed at different concentrations (120, 150, 180, 200, 250 and 300 mg/mL). Both the cartridge temperature and heated bed temperature were adjusted to always obtain the best resolution for each printing. Cartridge temperature was therefore selected depending on each recombinamer, always within a range of temperatures (9–11 °C) several degrees below

their respective Tt. By contrast, bed temperature was always set at 30 °C, to guarantee being always above Tt of the recombinamers.

Extrusion of the recombinamers was performed at velocity of 1 mm/s of the cartridge by using a 0.06 mm^3/s flow.

To determine the Pr parameter, optical images were obtained using a LEICA DMS 1000 digital microscope and images analysed using Image *J* software to determine the perimeter and area of the pores (n = 5).

2.4. Stability of the printed structures in an excess of aqueous medium

Cylinders with a diameter of 6 mm and height of 1.5 cm were designed.

A solution of each recombinamer was prepared, selecting the best printability obtained with the lowest concentration, as determined previously (250 mg/mL for Z-EI-ELR and S-EI-ELR and 180 mg/mL for the ZS-EI-ELR). After printing, the structures were immersed in 2 mL of PBS at 37 °C and maintained at this temperature. The structures were then placed into an incubator and pictures (NIKON D90) were taken at different times in order to monitor the evolution and stability of the hydrogels.

2.5. Rheological characterization

Rheological measurements were performed for the ZS-EI-ELR, which was dissolved, at different concentrations (120, 150, 180, 200, 250 and 300 mg/mL) 12 h before the experiments to ensure a complete dissolution into the PBS solvent.

A strain-controlled AR-2000ex rheometer (TA Instruments) with parallel plates of nonporous stainless steel was employed to perform rheological experiments in shear deformation mode. Measurements were performed using a temperature ramp, with the sample temperature being controlled and maintained using a Peltier device.

The ZS-EI-ELR was maintained for temperature homogenisation for 5 min at 4 °C before measurements, and a circular geometry of 40 mm diameter was used, ensuring that a minimum value of 1000 microns was always selected.

Flow measurements were performed to determine the evolution of the viscosity of the ZS-EI-ELR solution with shear rate. An initial conditioning step was set at a constant shear rate of 2 s^{-1} for 1 min. The shear rate was then swept from 1 to 1500 s^{-1} using a continuous ramp in a logarithmically ascending series of discrete steps. Specifically, 10 points were acquired for each order of magnitude, with the complete measurement taking 3 min.

Oscillatory measurements were also carried out. First, a solution of the ZS-EI-ELR in PBS was placed on the plate (40 mm diameter) at 4 °C and a temperature ramp from 4 to 37 °C was applied at a ramp rate of 5 °C/min, a frequency of 1 Hz and a strain amplitude of 0.5 %, which was established to be within the linear viscoelastic range. In situ gelation took place during the temperature ramp.

The dynamic shear modulus of the hydrogels was characterized at 37 °C using a strain and frequency sweep (plate diameter of 12 mm). A normal force was selected to prevent slippage. The dynamic strain sweep uses amplitudes ranging between 0.01 % and 30 % at a frequency of 1 Hz, while in the frequency sweep a range of 0.1–50 Hz was swept at a fixed strain (selected within the hydrogel linear region; specifically, a value of 0.5 % was chosen).

Rheological evaluation provided the storage modulus (G'), loss modulus (G") and complex viscosity magnitude $|\eta^*|$, ($|\eta^*| = |G^*|/\omega$, where $|G^*|^2 = (G')^2 + (G")^2$ is the complex module magnitude and ω is the angular frequency) as a function of strain amplitude or frequency.

2.6. Three-dimensional printing of the ZS-EI-ELR

A 180 mg/mL solution was selected as optimal for ZS-EI-ELR printing. The ZS-EI-ELR was prepared by dissolving pure lyophilized polymer in aqueous solution (PBS).

Scaffolds with a diameter of 6 mm were designed with 90° pores. Several scaffolds were printed using a blunt needle with a diameter of 0.25 mm and flux of 0.6 mm/s, decreasing the pore size until filament blending. Both ZS-EI-ELR and nivea cream as control [32] were tested (results shown in Figure S6).

The reliability of the ZS-EI-ELR printing was also demonstrated by printing different previously designed scaffold conformations. The conformation of the structures obtained, as well as the fibre arrangement, was observed by scanning electron microscopy (SEM).

2.7. Stability of the printed ZS-EI-ELR structures after lyophilisation and reconstitution

Stability of the printed ZS-EI-ELR structures was measured to determine the possibility of scaffold storage by lyophilisation. Thus, freshly printed scaffolds were stored at 37 °C for 24 h prior to cryogenization with liquid nitrogen and subsequent lyophilisation. Once structures had been dehydrated, they were reconstituted in PBS.

The width of the filaments and height and diameter of the scaffold were measured at each step to study conformational changes.

2.8. Cell culture and seeding

Human Foreskin Fibroblast (HFF-1) (ATCC, SCRC-1041) were expanded in DMEM 1X (4.5 g/L glucose, Corning) supplemented with 15 % fetal bovine serum and penicillin/streptomycin antibiotic solution. Cells were cultured at 37 °C at 90 % humidity and 10 % CO_2 atmosphere, changing the medium every 2 days.

Three independent experiments, each in triplicate, were performed for each test.

2.9. Cell seeding efficiency and cytotoxicity

The ZS-EI-ELR was extruded into a 96-well plate, forming a hydrogel at 37 °C. 20,000 HFF-1 cells were seeded onto the hydrogel disc using a volume of 30 μL. Cell-seeded scaffolds were incubated for 30 min in order to encourage cell adhesion prior to the addition of additional culture medium. To test seeding efficiency, the scaffolds were washed twice with PBS prior to addition of AlamarBlue® reagent at 30 min, 2 and 4 h. Fluorescence intensity emission was measured at 590 nm after excitation at 560 nm (SpectraMax M5e (Molecular Devices) microplate reader). The value obtained was converted into the number of cells by using calibration curves obtained using known numbers of HFF-1 cells seeded on 96-well plates.

Immunofluorescent analysis were also performed for the observation of the cell morphology at early cell attachment over the ZS-EI-ELR surface, where actin fibres (red), vinculin (green) and cell nuclei (blue) were stained. Cells were washed with PBS and fixed by addition of 4 % paraformaldehyde (PFA) in PBS for 10 min. After removal of the PFA, triton (1 % in PBS) was subsequently added on top of the scaffolds and incubated for 10 min to induce cell permeabilization. Fetal Bovine Serum (BSA - 1 %) was subsequently added as blocking solution for 30 min. Antivinculin rabbit monoclonal antibody (AlexaFluor® 488) (1:200) (Abcam) was used to study focal contact formation, meanwhile cell actin cytoskeletons were stained with Rhodamin phalloidin (1:60) (Invitrogen)

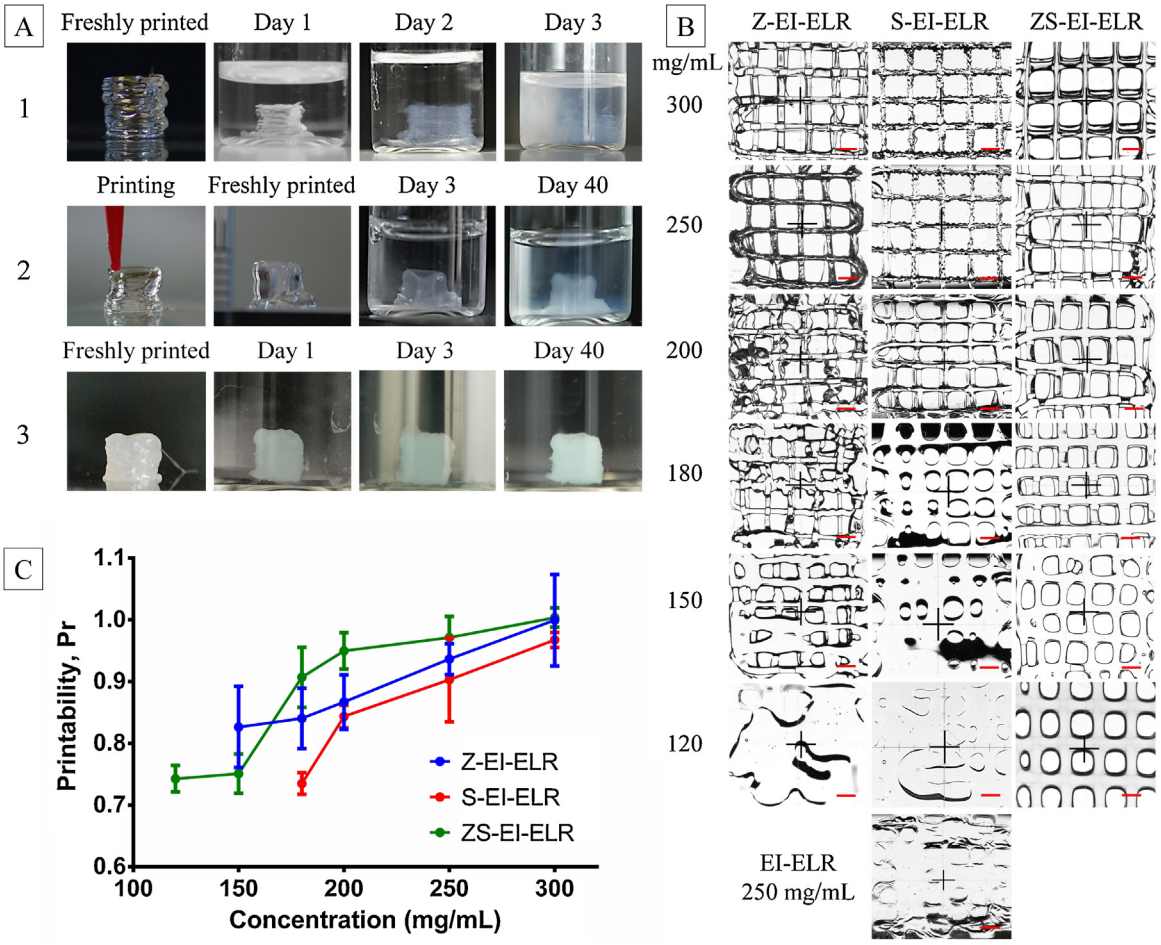

Fig. 3. (A) Pictures of structures printed using 1) Z-EI-ELR, 2) S-EI-ELR, and 3) ZS-EI-ELR, showing the stability over time. (B) Images of the printed Z-EI-ELR, S-EI-ELR, and ZS-EI-ELR structures at concentrations of 120, 150, 180, 200, 250 and 300 mg/mL, and EI-ELR at 250 mg/mL, all of them in PBS. Scale bar: 1 mm. (C) Calculated Pr values for the printed Z-EI-ELR, S-EI-ELR, and ZS-EI-ELR structures at concentrations of 120, 150, 180, 200, 250 and 300 mg/mL in PBS.

and DAPI (1:00,000) (Lonza) was used for the cell nuclei. A fluorescence inverted microscope (Nikon Eclipse Ti E) was used for the staining observation, where representative pictures were taken.

To measure the cytotoxicity, scaffolds with a diameter of 0.6 mm were printed and deposited onto 96-well plates. The scaffolds had a height of 0.5 mm and presented 1.2 mm, 90° square pores. The metabolic activity in the ZS-EI-ELR printed scaffold was assessed using AlamarBlue® reagent at 1, 3, 7, 14 and 21 days for scaffolds seeded with 20,000 HFF-1 cells. The mean fluorescence emission was calculated for each sample and normalized to the fluorescence for the unseeded control.

2.10. Viability of the printed ZS-EI-ELR cell-loaded bioink

6×10^6 HFF-1 cells were mixed into a 180 mg/mL final concentration of the ZS-EI-ELR in the cell culture media at 4 °C. Scaffolds with a diameter of 0.6 mm and height of 0.5 mm were printed under sterile conditions and designed to contain 1.2 mm, 90° square pores. Immediately after printing, scaffolds were placed into culture medium and incubated at 37 °C for a 21-day period. Live and dead stain (LIVE/DEAD Viability/Cytoxicity Assay Kit, Invitrogen) was performed over printed structures according to the manufacturer's instructions and cells were visualized using a Nikon eclipse Ti (Japan) fluorescence microscope, obtaining images at 4 h and 1, 3, 7, 14 and 21 days after printing. The percentage of living cells was calculated using imaging software (imageJ) taking into account the proportion of stained cells of each colour. Additionally, confocal images were taken, where cross sections of stained bioprinted structures at day 15 were observed. A confocal microscope Leica SP8 X coupled with an APO 10X/0.75 IMM CORR CS2 objective was used for this purpose. Taken images were analysed by using the Leica Application Suite X (LAS X) software.

In order to test the applicability of the printed process with other cell lines, Human umbilical vein endothelial cells (HUVECs) (Lonza, cc-2517) and Normal Human Adipose-Derived Mesenchymal Stem Cells (hMSCs) (ATCC, PCS-500-011) were used.

HUVECs were cultured in endothelial growth medium (EGM-2) supplemented with the EGM-2 SingleQuots Supplements required for their growth (Both purchased from Lonza). Incubation conditions were set at 37 °C and 5 % CO_2.

hMSCs were cultured in DMEM 1X (Corning, 1 g/L glucose) supplemented with 10 % fetal bovine serum and penicillin/streptomycin antibiotic solution. Cells were incubated at 37 °C, 90 % humidity and 10 % CO_2 atmosphere.

For this experiments, the ZS-EI-ELR was dissolved in the corresponding cell media, and cells were loaded by achieving a final concentration of 180 mg/mL of the bioink (a number of 7×10^6 HUVEC cells per millilitre and 6×10^6 hMSCs cells per millilitre was used). Fibres of the different cell lines were bioprinted into different experiments and viability and cell morphology were tested in the same way as explained for the HFF-1 cell line, until 7 days of incubation time.

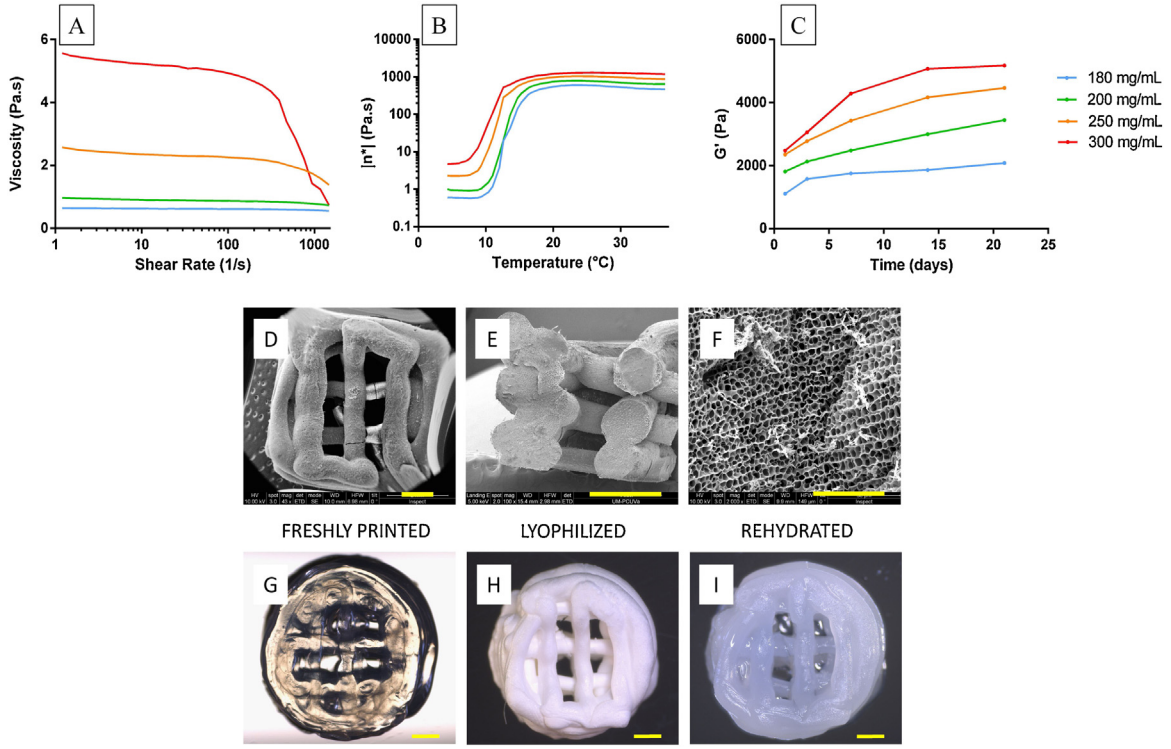

Fig. 4. A) Plots of viscosity vs. shear rate for the ZS-EI-ELR. B) Evaluation of the viscosity of the ZS-EI-ELR with temperature. C) Evolution of the storage modulus (G') with time. D), E), F) Printed scaffolds observed by SEM at different magnifications. Scale bar for d) and e) 1 mm; for f) 50 μm. G), H), I) Images of a printed scaffold after printing, lyophilisation and rehydration, respectively. Scale bar: 1 mm.

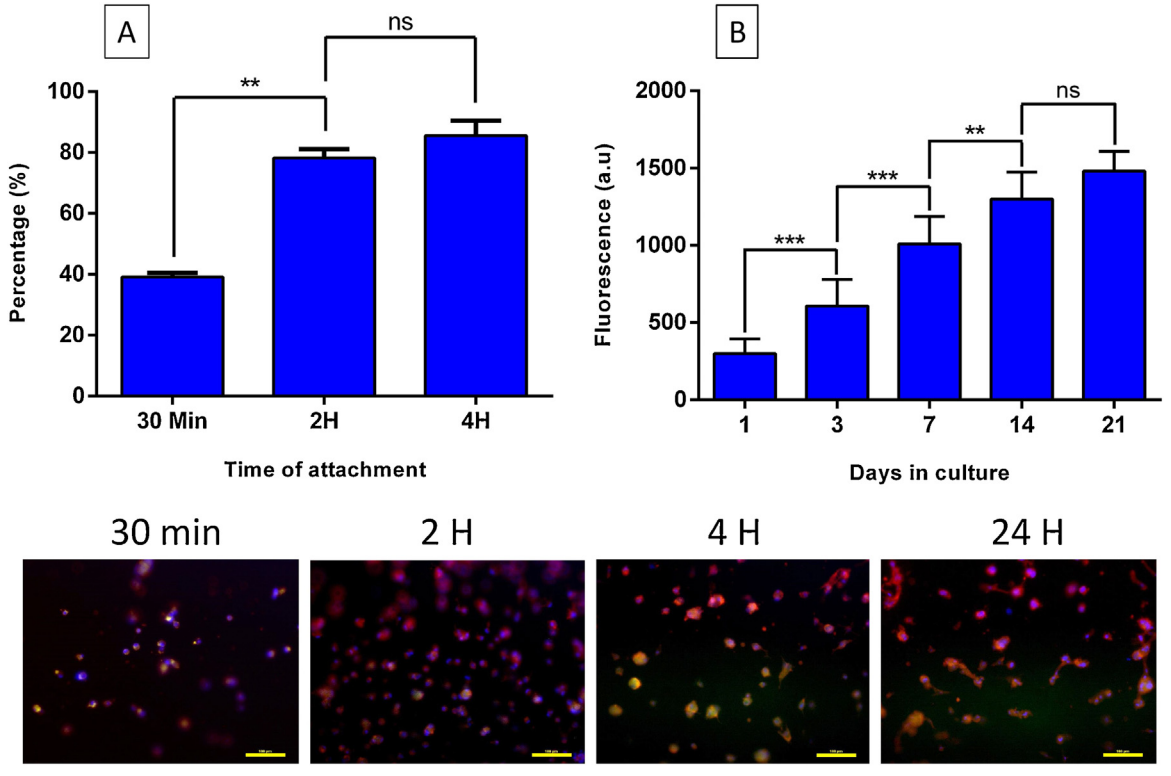

Fig. 5. A) Percentage of HFF-1 seeding efficiency on a ZS-EI-ELR hydrogel surface. B) Alamar blue reduction of cells seeded upon a ZS-EI-ELR printed scaffold. C) Immunostaining of actin (red), vinculin (green), and nuclei (blue) of HFF-1 cells at early adhesion for different time points (30 min, 2 h, 4 h and 24 h) over ZS-EI-ELR hydrogels. Scale bar 100 μm (ns $P > 0.05$; *$P < 0.05$; **$P < 0.01$; ***$P < 0.001$; ****$P < 0.0001$).

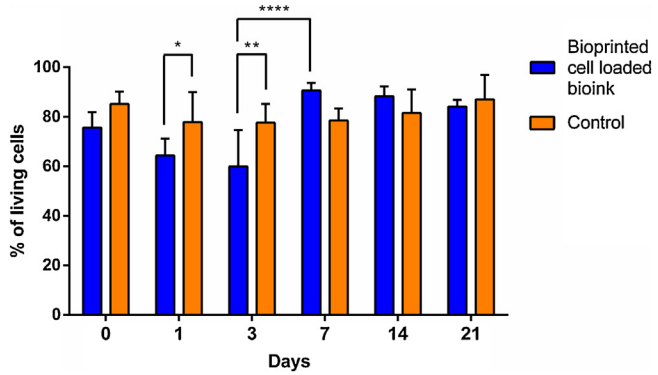

Fig. 6. Viability of HFF-1 cells loaded into 3D printed constructs during static culture for 21 days. Deposited cell loaded ZS-EI-ELR bioink was used as control. (ns P > 0.05; *P < 0.05; **P < 0.01; ***P < 0.001; ****P < 0.0001).

2.11. Cell morphology and spreading

Morphology of HFF-1 cells loaded onto ZS-EI-ELR bioink printed scaffolds was observed by inverted microscopy. Fluorescent staining of F-actin and cell nuclei was performed using DAPI/Phalloidin (Invitrogen), respectively. The printed scaffolds were previously washed with PBS and fixed, permeabilized and blocked as explained in Section 2.9, but increasing the incubation times (PFA, 1 h; triton 1 % in PBS), 30 min; (BSA - 1 %), 1 h). Reagents were diluted in PBS containing 1 % FBS at 1:60 (Phalloidin) and 1:50 (DAPI) v/v. Phalloidin was incubated for 30 min and washed with PBS, whereas DAPI was added for two minutes. The stained scaffolds were then washed three times with PBS before visualization.

2.12. Statistical methods

Each experiment was performed in triplicate. For statistical analysis of the data, the Graph Pad software was used. The mean and standard deviation were calculated and tested for normality using a D'Agostino-Pearson test and for homoscedasticity. Results were normalized when needed. Assuming a Gaussian distribution, a 2-way ANOVA was applied for the data, followed by a Tukey's multiple comparison test between groups. When only two groups needed to be compared, a student's *t*-test was performed.

Obtained values were represented by their significance level: ns P > 0.05; *P < 0.05; **P < 0.01; ***P < 0.001; ****P < 0.0001.

3. Results and discussions

3.1. Design, construction and characterization of the novel ZS-EI-ELR

The amino acid sequence of the novel designed recombinamer ZS-EI-ELR can be found in Table 1, as well as the sequence of previously developed recombinamers that have been already reported and will be used as control. Both Z-EI-ELR [28] and S-EI-ELR [29] show a similar structure to the ZS-EI-ELR but lacks from the silk domain and the zipper domain respectively (Fig. 2). The EI-ELR [27] is also taken into account as it lacks both reinforcement sequences.

DNA sequencing and restriction mapping analysis of the ZS-EI-ELR showed the correctness of the gene construction process (data not shown). Once the recombinant plasmids were cloned into *escherichia coli*, positive clones showing the highest ELRs expression levels were stored as glycerol stocks for their indefinitely production.

Recombinamer was successfully bioproduced and purified following an inverse temperature cycling protocol [33]. After lyophilisation, production yields of around 150 mg per litre of bacterial culture were achieved. The obtaining product was characterized by SDS-PAGE (Figure S1), amino-acid composition analysis (Table S1), mass spectrometry (MALDI-TOF, Figure S2), ^{1}H NMR, (Figure S3) and DSC (Figure S4). All the analyses confirmed the purity and correctness of the biosynthetic process in terms of sequence and molecular mass (see Supplementary material).

3.2. Printability characterization

As a result of the developed innovative molecular design of the ZS-EI-ELR, the following dynamic cascade behaviour is expected during the printing process in a kind of domino effect:

An initial increase in temperature from below to above the transition temperature of the hydrophobic elastin-like blocks triggers hydrophobic assembly of the amphiphilic EI-blocks, thus resulting in a rapid sol-gel transition. This first gel state is then further reinforced by the subsequent and progressive emergence of two new intramolecular interactions that generate two additional supramolecular structures, namely Leu-zippers [28] and β-sheets, formed by the Z and silk-like blocks, respectively. The hypothesis of this work is that, as intermolecular interactions are essentially nonexistent when the ELR solution is kept below the Tt of the I block, the system behaves as a solution with low viscosity and high injectability. If deposited on a substrate that is kept above Tt, the sol rapidly changes to a gel and, although this initial gel state formed simply by the weak hydrophobic association of the I blocks is unstable and not suitable per se for 3D printing, this hydrophobic association triggers the intermolecular interaction of the remaining Z and silk-like blocks, as reported previously [28]. In a relatively rapid manner, the first and, somewhat more slowly, second gel states will stabilize and improve the mechanical characteristic of the final gel to achieve a stable system that maintains its size and shape for long periods irrespective of whether the gel is kept immersed in an aqueous medium.

To test our hypothesis, printability was the first parameter to measure.

As the unique behaviour of our ink recombinamer is related to the ITT, a special cooling cartridge was designed, printed using a stereolithography printer and implemented in the 3D bioprinter. This cartridge was used to regulate the temperature of the ZS-EI-ELR in the reservoir, before deposition onto a heated bed to provide the required fast transition.

Printability was studied at different ZS-EI-ELR concentrations ranging from 120 to 300 mg/mL. To test the need for inclusion of both the Leu-Zipper and silk sequences into the ZS-EI-ELR, a Zipper-containing elastin-like recombinamer lacking silk-like domains, known as Z-EI-ELR [28], and a silk-elastin like recombinamer lacking Leu-Zippers, known as S-EI-ELR [29], were also printed in the same conditions (their respective amino-acid sequences are shown in Table 1).

Filaments of ZS-EI-ELR were deposited with high precision, thus allowing the formation of structural matrices that show contour accuracy in time and space (Fig. 3B). In all cases of ZS-EI-ELR printing, the deposited fibres were smooth and linear. A Pr value was calculated to determine how the printed structure differs from the designed one (Fig. 3C). When this value ranges from 0.9 to 1.1, the 3D printed structures exhibit correctly deposited fibres with controlled printability. Moreover, the fibres did not fuse when printed on top of each other, thus resulting in mechanical stability and avoiding structural collapse. Higher Pr values were obtained at concentrations higher than 180 mg/mL.

In comparison to the printability of ZS-EI-ELR, Z-EI-ELR results in globular and less homogenous fibres, although fibre collapse is also avoided at 180 mg/mL (Fig. 3B), thus confirming that the Zipper sequence plays a role in the resolution of fibre deposition. Printing

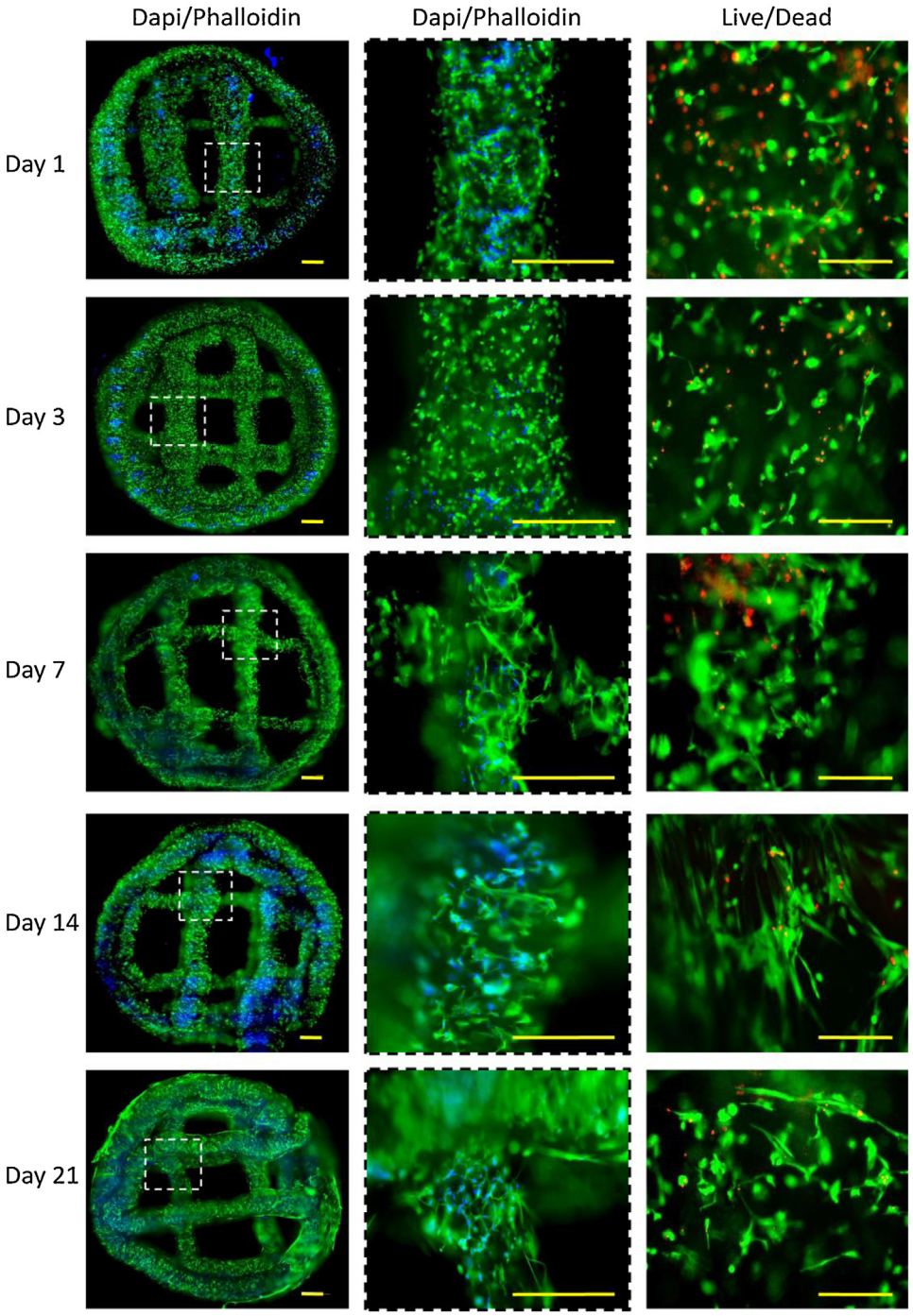

Fig. 7. Microscope images of ZS-EI-ELR bioink scaffolds loaded with HFF-1. Dapi/Phalloidin staining of a complete printed structure and a magnified zone into the middle, and L/D assays over a 21-day culture. Scale bar for dapi/phalloidin: 500 μm; for live/dead: 200 μm.

with S-EI-ELR results in an irregular deposition above 200 mg/mL, with the structure not being maintained at lower concentrations. The Pr values for these two recombinamers are also lower than those for the ZS-EI-ELR, as shown in Fig. 3C.

As a control, an EI recombinamer was also tested at high concentration (250 mg/mL) and found to be unable to form stable fibres when printed alone, thus showing the need for the addition of reinforcement gelation sequences, as expected.

The fact that better Pr values were obtained into the recombinamers with the Zipper domain included proves the second part of our hypothesis. The inclusion of this reinforcement seems to avoid early filament collapsing after printing.

3.3. Stability of the printed structures in excess of aqueous medium

In addition to an improved printability, constructs printed with ZS-EI-ELR showed vertical stability even when immersed in a fluid, with both freshly printed and incubated scaffolds being found to retain their structure for at least 40 days after immersion in an aqueous medium (Figure 3A-3).

This was not the case for the Z-EI-ELR constructs despite the fact that they showed early reliability that allowed the printing of height-stable structures (Figure 3A-1). The S-EI-ELR construct, in turn, was unable to retain its structure even in the early stages

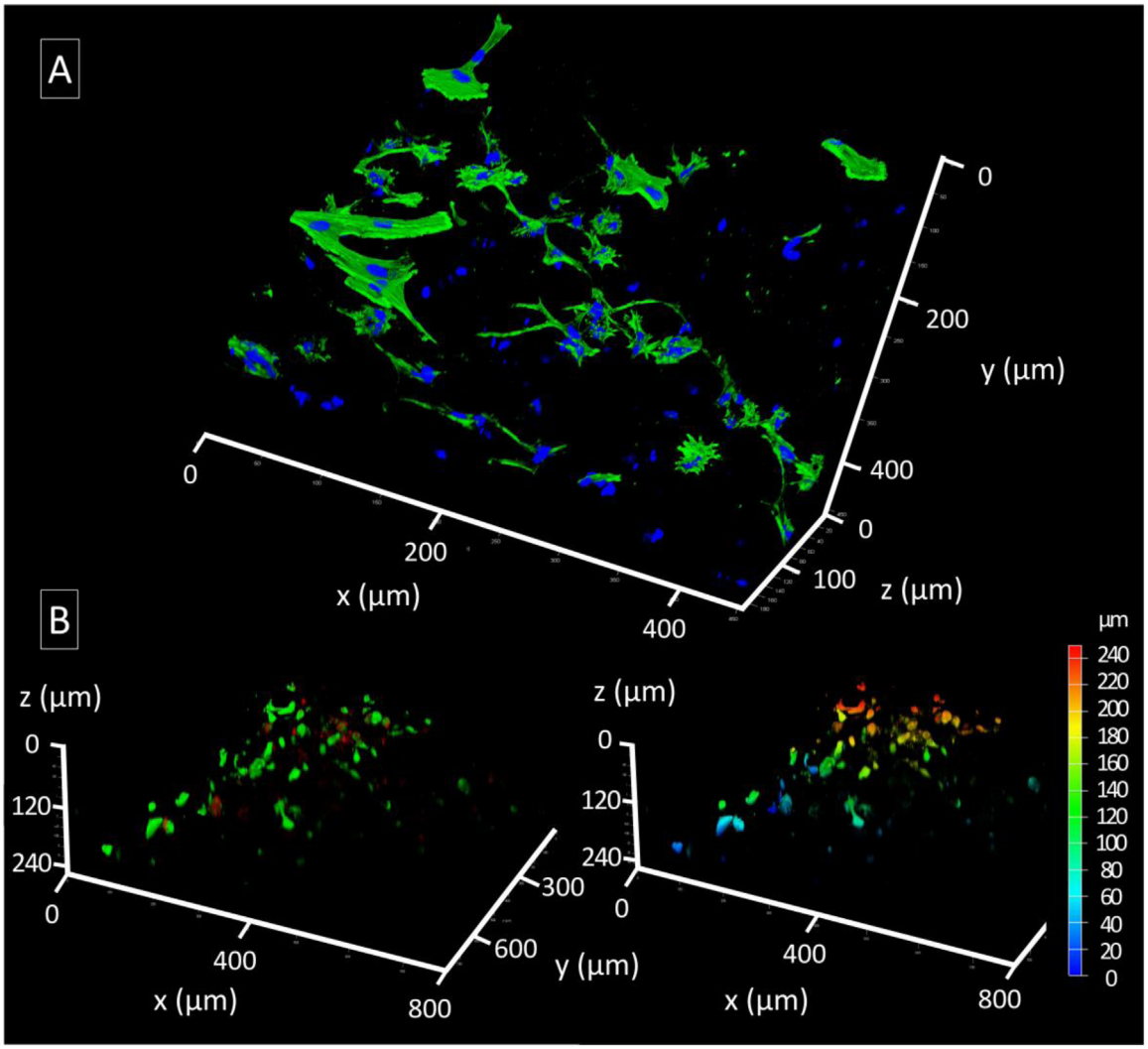

Fig. 8. Confocal images of the staining of a cross-section of the bioprinted ZS-EI-ELR bioink loaded with HFF-1 cell. A) actin fibers (green) and cell nucleus (blue), B) live cells (green) and dead cells (red) places distributed within the scaffold. A depth colour coding is included.

(Figure 3A-2) as the amphiphilic EI tetrablock is solely responsible for initial crosslinking and shows some degree of fluency as the silk-like block requires more time to freeze the printed structures. The need for inclusion of both the zipper and silk sequences within the chain of the ZS-EI-ELR is therefore clear as both reinforcement sequences working in cascade seem to endow the printed structure with a specificity during gelation that cannot be achieved by the same sequences acting separately. Our rationale for construction of the ZS-EI-ELR ink construction has been thus proved to be correct.

3.4. Rheological properties of the ZS-EI-ELR

Once printability had been tested, the behaviour of the ZS-EI-ELR when subjected to extrusion also needed to be tested as the physical properties of the ink appear to have an effect on scaffold deposition and, therefore, resolution. As such, rheological experiments were performed to simulate the printing process and to help to understand how the forces ejected govern performance of the ink. The ZS-EI-ELR was initially characterized by measuring the dependence of viscosity on shear rate. A wide range of shear rates were used to cover the different shear rate conditions found during extrusion (Fig. 4A).

The viscosity of ZS-EI-ELR increases with concentration, reaching a maximum of 5 Pa.s at 300 mg/mL and a minimum of 0.2 Pa.s at 180 mg/mL. Whereas no dependence on shear rate is observed at low concentration (Newtonian fluid), an evolution of the viscosity with shear rate is detected at higher concentrations for shear rates higher than 400 s^{-1}. This latter behaviour corresponds to a Bingham plastic.

In contrast to many other developed inks, which exhibit high viscosity when low shear forces are applied [34,35], shear thinning is not a required parameter to achieve good printability in ZS-EI-ELR. This is because, in this case, the rapid viscosity increase that enables good printability is guided by the ITT instead of by shear forces. The lower initial viscosity of the ZS-EI-ELR compared to others also facilitates its handling.

Gelation is a key aspect of ZS-EI-ELR fibre deposition (Figure S7) as it depends on the ITT. The initial viscosity of the ZS-EI-ELR stored in the cartridge can be controlled by increasing the temperature. To study this parameter, oscillatory measurements were performed for a temperature ramp from 4 to 37 °C. Changes in the conformation of ZS-EI-ELR were observed by plotting G' and G" vs temperature (Figure S8), and the complex viscosity magnitude was extracted from the complex modulus magnitude (Fig. 3B). The lowest available viscosity of 0.5 and 2.2 Pa.s for concentrations of 180 and 250 mg/ml, respectively, was obtained at temperatures lower than 12 °C. Viscosity then increased with temperature up to a temperature of 25 °C, where the polymer gels with

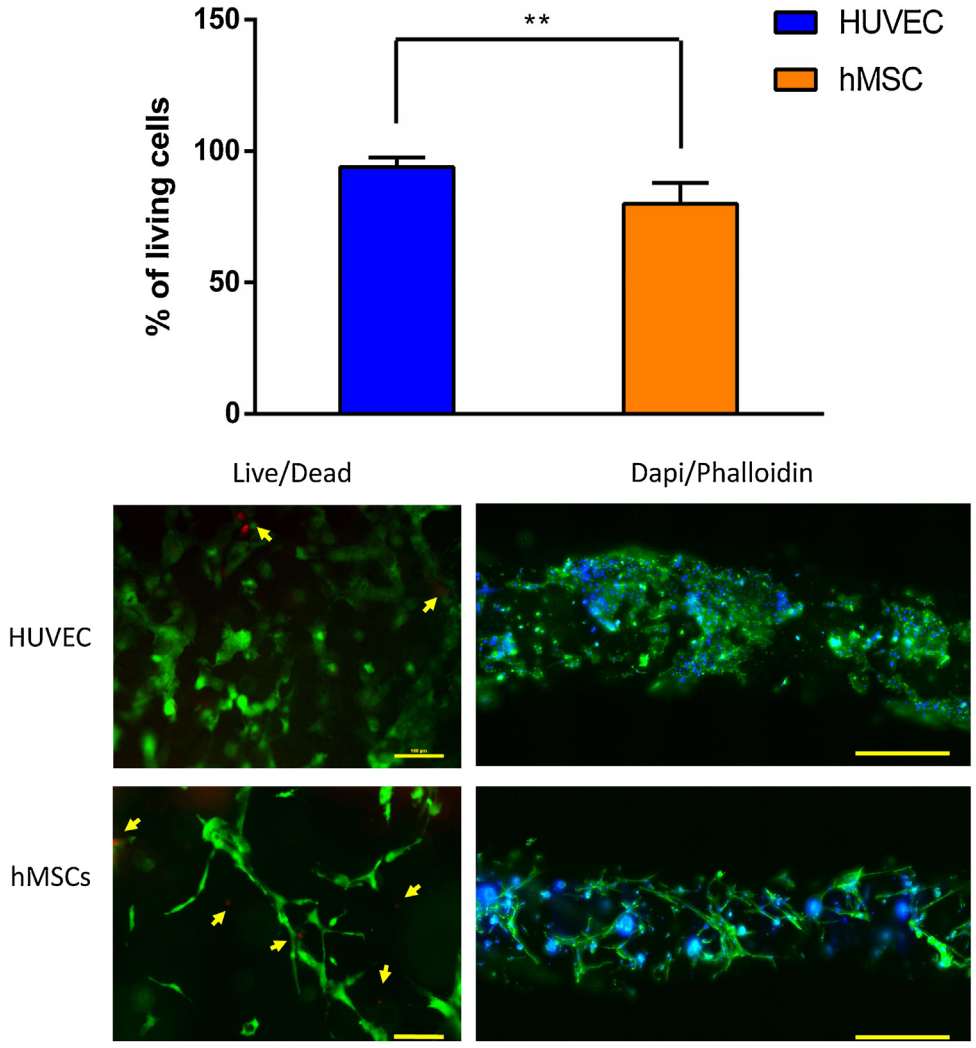

Fig. 9. Microscopy images of live/dead and dapi/phalloidin staining for HUVEC and hMSCs cells loaded into the ZS-EI-ELR and bioprinted. For dapi/phalloidin staining, the maximum intensity of the Z stacking is shown. Scale bar for the live/dead: 100 μm; for dapi/palloidin XXX. Viability of the bioprinted cells was also measured and represented in the graph above. (ns $P > 0.05$; *$P < 0.05$; **$P < 0.01$; ***$P < 0.001$; ****$P < 0.0001$).

a viscosity of around 600 Pa.s and some degree of concentration-dependence. To ensure better fibre resolution, the temperature of the cartridge should be set to slightly lower than the ITT (Figure S4).

Annealing of the hydrogels formed with the ZS-EI-ELR was studied over time, showing that maturation of the β-sheet arrangements enhances the stability of the structures. Evolution of the storage modulus G' was recorded for different curing times. As can be seen in Fig. 4C, the storage modulus was higher at each measuring time as concentration increased. Moreover, its value increased with time during the experiment, with this increase being more marked over the first 7 days and then becoming less pronounced, thus suggesting completion of β-sheet formation. The final G' stiffness measured corresponds with the measurement of the natural stiffness, ranging from ~100 Pa for very soft tissues such as fat or brain to >10,000 Pa for muscle.

Given the results obtained, a 180 mg/mL ZS-EI-ELR solution was selected as optimal. This concentration was the lowest that provides linear, smoothly printed fibres that avoid collapse. In addition, the lower viscosity of the 180 mg/mL ZS-EI-ELR facilitates its handling and reduces the shear forces required for extrusion. Using this concentration, larger internal pores were also expected than for higher concentrations.

3.5. Three dimensional printing of the ZS-EI-ELR ink

For a hydrogel to be considered as a good ink candidate, it needs to show both adequate mechanical properties and to be able to be printed with resolution, versatility and reproducibility. In this regard, ZS-EI-ELR allows the printing of scaffolds with various conformations, preserving the structure of the computer-designed scaffold, as can be seen in the pictures and SEM images (Fig. 4D, 4E, 4 F). Fibres were found to be distributed one on top of the other, merging sufficiently to provide matrix shape-retention without collapsing, even when printed without a support for small distances. The porosity of the surface was also demonstrated, thus providing anchorage points for cell interactions.

From a practical point of view, a method for ZS-EI-ELR printed matrix preservation was studied, which is an interesting characteristic to be considered for production of a cell-free scaffold that will subsequently be used for tissue-engineering purposes. With this in mind, scaffolds were subjected to cryopreservation and lyophilisation (Fig. 4G, 4H, 4I). Subsequent measurement of the height, breadth and filament width of the structures revealed no statistically significant differences between them when freshly printed, lyophilized or rehydrated, thus suggesting that this process

does not affect the internal structure of the matrix when rehydrated.

3.6. Cell seeding efficiency and citotoxicity

Ideally, these printed scaffolds must be able to support cell attachment and proliferation. As such, the HFF-1 cell line was used to test cell-matrix interactions. The ability to promote cell adhesion was evaluated initially to determine the quantity of cells that are adhered to the ZS-EI-ELR matrix. Thus, shortly after cell seeding into a moulded ZS-EI-ELR hydrogel, 39.14 % of the cells were adhered to the surface, with this value increasing to 78.53 % after two hours and reaching 86.03 % after 4 h (Fig. 5A). Both the irregular surface of the matrix and the inclusion of RGD sites in the ZS-EI-ELR amino acid chain seem to effect the early stages of adhesion, and it is well known from the literature that cell attachment is influenced by several factors, including inclusion of the RGD peptide [36,37].

A staining of the HFF-1 cells seeded on top of the ZS-EI-ELR hydrogels for actin skeleton (red), cell nuclei (blue) and vinculin (green), revealed their morphological shape, spreading, cytoskeletal reorganization and focal adhesion distribution (Fig. 5C) for 30 min, 2, 4, and 24 h of incubation.

By washing with PBS before staining, we ensured that non-adhered cells were discarded, which means that in spite of their noticed rounded shape, observed cells over the matrix were attached to its surface. Lesser cells were observed after 30 min over the surface in comparison with the amount of cells attached after 2 or 4 h. This observation is in line with the data obtained by the measurement of the cell seeding efficiency.

Cells remained mostly globular at 30 min, and 2 h, showing both actin and vinculin initially circumscribed to the perinuclear zone. At four hours, small irregularities in cell shape was first observed, where some cells started to spread their actin filaments. Finally, after the first 24 h, several cells showed an elongated shape, where the vinculin was overlapped with the actin filaments.

Cytocompatibility of the ZS-EI-ELR was assessed using the AlamarBlue assay (Fig. 4B), which showed an increase in metabolic activity, especially within the first 2 weeks, most likely due to the increase in the number of cells. Moreover, the viability of the cells remained high throughout the 4 weeks of culture. An analysis of variance (ANOVA) revealed statistically significant differences in proliferation rate between culture days, with the exception of day 21. Thus, cells maintain their normal metabolic activity when seeded upon the structures, thus demonstrating a friendly environment for cell proliferation.

3.7. Viability and cell morphology after cell loaded 3d bioprinting of ZS-EI-ELR

To demonstrate the utility of this material as a bioink for tissue engineering, in addition to promoting cell attachment and providing a non-toxic environment for cell proliferation, we need to ensure cell support throughout the printing process. To that end, the ZS-EI-ELR was loaded with fibroblast cells and the effect of the shear forces exerted was measured by imaging using live/dead staining (Figs. 6 and 7). The obtained results were compared with the control cell loaded ZS-EI-ELR not subjected to the bioprinting process.

The ZS-EI-ELR bioink showed a cell viability of 75.61 % when printed using a 0.25 diameter needle 4 h after printing. Non-significant difference with respect to the control was found at early bioprinting.

By contrast, although viability is maintained by the control during the 21-days incubation time, the amount of viable cells within the printed sample decreased slightly to 59.91 % after three days of cell culture. After the first days of incubation, viability subsequently increased and remained high thereafter, showing values comparable to the control samples. This initial decreasing into viability demonstrated by the ZS-EI-ELR bioink has been previously reported for other bioprinted systems and it is attributed to the mechanical forces applied by the 3D bioprinted process, which may contribute to alter the natural cell behaviour [38] or even to induce cell death via membrane disruption [39].

Morphology of the cells was also characterized by dapi/phalloidin staining to investigate cell spreading and cytoskeletal reorganization over a 21-day culture period. HFF-1 cells were found to be homogeneously distributed within the printed ELR scaffold (Fig. 7). Cell morphology was rounded in the early stages, as was also observed for the early attachment experiment. At day 3, most of the cells subsequently started to develop their characteristic filamentous shape, being completely spread at 7 days, where they revealed clear nuclei and displayed a longitudinal profile, forming aggregates along the length of the structure. After 21 days of culture, the structure still maintained its ability to support cell growth and proliferation.

Rounded cell morphology during the first three days of culture was expected as previously determined also into the cell adhesion assay thus it did not affect negatively on their viability and proliferation. One of the main reasons for this behaviour is the stiffer three-dimensional architecture of the hydrogel, formed by internal porosity in which the cells occupy the maximum space. In fact, it is reported that in 3D gels, cells retard their spreading in expense of proteolytically cleavage the physical scaffold [40]. Moreover, it is known that matrix stiffness plays an important role into cell behaviour, guiding motility, tension and even regulation of lineage changes [41]. As cell proliferation is enhanced in stiffer gels, observation of more spread cells at long incubation times, can also be the result of the increment of stiffness that suffer the scaffold from the maturation of the β-sheet interactions [41].

On the other hand, the introduction of RGD sequences into the ZS-EI-ELR seems to improve the spreading rate of the HFF-1 cell line, as this RGD domain acts as an anchorage point for the cells to attach and disseminate within the scaffolds [42], indeed, higher density of RGD has been linked with higher cell motility and spreading [43]. So, in future research, the introduction of a higher quantity of RGDs motifs into the ZS-EI-ELR sequence could improve cell behaviour.

Confocal microscope coupled with the 10X objective allowed the study of the distribution and viability of the cells within the bioprinted structures, enabling a maximum depth penetration of 300 μm. Cross-section observations of the bioprinted structures over the Z axis revealed the porous structure of the gel, where the cells were placed. A 10 μm layer of material was found at the surface of the scaffold. Once the laser surpasses this outer layer, cells seem to be distributed evenly towards the interior showing an elongated shape, with the actin fibres distributing into the three dimensions, as can be seen into the actin/nucleus staining (Fig. 8A). Cells situated in the surface of the material showed a more elongated shape that the ones in the inner parts. On the other hand, population was maintained over the range of depth penetrated, showing the same distribution of live and dead cells, which means that cells remain viable within the inner part of the structure (Fig. 8B). In the light of the observed results, it can be deduced that nutrients are free to pass throughout the scaffold, where the cells are placed, preserving them alive. Having into account that the printed scaffold in itself has been designed with macroporous, showing fibres from 200 to 500 μm even the more internally placed cells are supposed to be irrigated by cell culture media.

Similar results were obtained for the bioprinting of the ELR bioink loaded with HUVEC or hMSCs cells (Fig. 9). By using the same printing conditions and ZS-EI-ELR concentration, viability into the bioink remained high for both cell lines at 7 days of fibres incubation. Morphology was also assessed by showing spreading for the

majority of the cells in both cases, as noticed also for the HFF-1 cell line at the same days of incubation. As HUVEC cells are smaller and do not show a fibrillary shape, as it happens with the HFF-1 or the hMSCs, they seem to respond better to the internal structure of the printed scaffold, even exhibiting cell aggregates.

It is important to remark that the properties of the developed ELR bioink can be enhanced by the introduction of other relevant peptide-based biological cues within its designed chain, which makes this ZS-EI-ELR bioink to be positioned as a very advanced tool. As an example, several domains have been successfully included into other kind of ELR developed for tissue engineering that can be considered, such as other cell-adhesion sequences as the REDV [44], responsive for HUVEC adhesion, or the IKVAV [45] for the sustaining of neuron attachment and growth. Also metalloproteinase cleavage sites [46] or vascular endothelial growth factor (VEGF) can be contemplated.

4. Conclusion

A novel advanced bioink has been molecularly designed on the basis of a protein-based material, with molecular programing of a complex, three-stage gelation process. This ELR-based bioink successfully overcomes the most relevant limitations found in other natural and synthetic bioinks.

Both the mechanical and printability properties underline the potential of this novel bioink as regards the generation of reliable structures based on 3D bioprinting by achieving this complex structural design. Additionally, the adequate extracellular environment that these new bioink provide for cell growth and proliferation has been confirmed.

In addition to their proven structural and biological properties, the synthetic production of the ZS-EI-ELR favors batch-to-batch homogeneity, thus removing one of the major drawbacks of natural bioinks. Moreover, this will also enable future tuneability given the ability to incorporate sequences of interest within the amino acid chain that may lead to innovative properties and bioactivities, thereby allowing the creation of tissue tailored bioinks.

Declaration of Competing Interest

The authors declare that there is no conflict of interest.

Acknowledgements

The authors are grateful for funding from the Spanish Government, [MAT2015-68901-R, MAT2016-78903-R, RTC-2018-096320-B-C22], Junta de Castilla y León [VA317P18], European Commission [Interreg V A España Portugal POCTEP (0624_2IQBIONEURO_6_E)] and Centro en Red de Medicina Regenerativa y Terapia Celular de Castilla y León. The authors also thank also R. García and J. Gutiérrez for their kind assistance.

Appendix A. Supplementary data

Supplementary material related to this article can be found, in the online version, at doi:https://doi.org/10.1016/j.apmt.2019.100500.

References

[1] E.B. Luiz, C.C. Juliana, M. Vijayan, L.C. Ana, S.B. Nupura, A.A. Wesleyan, Z. Pinar, E.V. Nihal, M.G. Amir, R.D. Mehmet, K. Ali, Direct-write bioprinting of cell-laden methacrylated gelatin hydrogels, Biofabrication 6 (2014), 024105.
[2] K. Nair, M. Gandhi, S. Khalil, K.C. Yan, M. Marcolongo, K. Barbee, W. Sun, Characterization of cell viability during bioprinting processes, Biotechnol. J. 4 (2009) 1168–1177.
[3] K. Holzl, S. Lin, L. Tytgat, S. Van Vlierberghe, L. Gu, A. Ovsianikov, Bioink properties before, during and after 3D bioprinting, Biofabrication 8 (2016), 032002.
[4] C. Mandrycky, Z. Wang, K. Kim, D.H. Kim, 3D bioprinting for engineering complex tissues, Biotechnol. Adv. 34 (2016) 422–434.
[5] N.E. Fedorovich, J. Alblas, J.R. de Wijn, W.E. Hennink, A.J. Verbout, W.J. Dhert, Hydrogels as extracellular matrices for skeletal tissue engineering: state-of-the-art and novel application in organ printing, Tissue Eng. 13 (2007) 1905–1925.
[6] L. Hyungseok, J.Y. James, K. Hyun-Wook, C. Dong-Woo, Investigation of thermal degradation with extrusion-based dispensing modules for 3D bioprinting technology, Biofabrication 8 (2016), 015011.
[7] C.C. Chang, E.D. Boland, S.K. Williams, J.B. Hoying, Direct-write bioprinting three-dimensional biohybrid systems for future regenerative therapies, J. Biomed. Mater. Res. Part B Appl. Biomater. 98B (2011) 160–170.
[8] C.M. Smith, A.L. Stone, R.L. Parkhill, R.L. Stewart, M.W. Simpkins, A.M. Kachurin, W.L. Warren, S.K. Williams, Three-dimensional bioassembly tool for generating viable tissue-engineered constructs, Tissue Eng. 10 (2004) 1566–1576.
[9] R. Censi, W. Schuurman, J. Malda, G. di Dato, P.E. Burgisser, W.J.A. Dhert, C.F. van Nostrum, P. di Martino, T. Vermonden, W.E. Hennink, A printable photopolymerizable thermosensitive p(HPMAm-lactate)-PEG hydrogel for tissue engineering, Adv. Funct. Mater. 21 (2011) 1833–1842.
[10] W.R. Gray, L.B. Sandberg, J.A. Foster, Molecular model for elastin structure and function, Nature 246 (1973) 461–466.
[11] R.S. Rapaka, D.W. Urry, Coacervation of sequential polypeptide models of tropoelastin, Int. J. Pept. Protein Res. 11 (1978) 97–108.
[12] D.W. Urry, T.L. Trapane, K.U. Prasad, Phase-structure transitions of the elastin polypentapeptide–water system within the framework of composition–temperature studies, Biopolymers 24 (1985) 2345–2356.
[13] D.E. Meyer, A. Chilkoti, Genetically encoded synthesis of protein-based polymers with precisely specified molecular weight and sequence by recursive directional ligation: examples from the elastin-like polypeptide system, Biomacromolecules 3 (2002) 357–367.
[14] A. Sánchez-Ferrero, Á. Mata, M.A. Mateos-Timoneda, J.C. Rodríguez-Cabello, M. Alonso, J. Planell, E. Engel, Development of tailored and self-mineralizing citric acid-crosslinked hydrogels for in situ bone regeneration, Biomaterials 68 (2015) 42–53.
[15] H. Wang, L. Cai, A. Paul, A. Enejder, S.C. Heilshorn, Hybrid elastin-like polypeptide-polyethylene glycol (ELP-PEG) hydrogels with improved transparency and independent control of matrix mechanics and cell ligand density, Biomacromolecules 15 (2014) 3421–3428.
[16] S. Ravi, J.M. Caves, A.W. Martinez, C.A. Haller, E.L. Chaikof, Incorporation of fibronectin to enhance cytocompatibility in multilayer elastin-like protein scaffolds for tissue engineering, J. Biomed. Mater. Res. A. 101 (2013) 1915–1925.
[17] D.W. Urry, T.M. Parker, M.C. Reid, D.C. Gowda, Biocompatibility of the Bioelastic Materials, Poly(GVGVP) and Its γ-Irradiation Cross-Linked Matrix: Summary of Generic Biological Test Results, J. Bioact. Compat. Polym. 6 (1991) 263–282.
[18] D.W. Urry, Free energy transduction in polypeptides and proteins based on inverse temperature transitions, Prog. Biophys. Mol. Biol. 57 (1992) 23–57.
[19] L. Martín, F.J. Arias, M. Alonso, C. García-Arévalo, J.C. Rodríguez-Cabello, Rapid micropatterning by temperature-triggered reversible gelation of a recombinant smart elastin-like tetrablock-copolymer, Soft Matter 6 (2010) 1121–1124.
[20] C. Vinson, M. Myakishev, A. Acharya, A.A. Mir, J.R. Moll, M. Bonovich, Classification of human B-ZIP proteins based on dimerization properties, Mol. Cell. Biol. 22 (2002) 6321–6335.
[21] C.R. Vinson, T. Hai, S.M. Boyd, Dimerization specificity of the leucine zipper-containing bZIP motif on DNA binding: prediction and rational design, Genes Dev. 7 (1993) 1047–1058.
[22] X.-X. Xia, Q. Xu, X. Hu, G. Qin, D.L. Kaplan, Tunable self-assembly of genetically engineered silk–Elastin-like protein polymers, Biomacromolecules 12 (2011) 3844–3850.
[23] M. Bongio, J.J. van den Beucken, M.R. Nejadnik, S.C. Leeuwenburgh, L.A. Kinard, F.K. Kasper, A.G. Mikos, J.A. Jansen, Biomimetic modification of synthetic hydrogels by incorporation of adhesive peptides and calcium phosphate nanoparticles: in vitro evaluation of cell behavior, Eur. Cell. Mater. 22 (2011) 359–376.
[24] J.A. Rowley, G. Madlambayan, D.J. Mooney, Alginate hydrogels as synthetic extracellular matrix materials, Biomaterials 20 (1999) 45–53.
[25] J. Reguera, A. Fahmi, P. Moriarty, A. Girotti, J.C. Rodríguez-Cabello, Nanopore formation by self-assembly of the model genetically engineered elastin-like polymer [(VPGVG)2(VPGEG)(VPGVG)2]15, J. Am. Chem. Soc. 126 (2004) 13212–13213.
[26] J.C. Rodríguez-Cabello, A. Girotti, A. Ribeiro, F.J. Arias, Synthesis of genetically engineered protein polymers (recombinamers) as an example of advanced self-assembled smart materials, in: M. Navarro, J.A. Planell (Eds.), Nanotechnology in Regenerative Medicine: Methods and Protocols, Humana Press, Totowa, NJ, 2012, pp. 17–38.
[27] L. Martín, E. Castro, A. Ribeiro, M. Alonso, J.C. Rodríguez-Cabello, Temperature-Triggered Self-Assembly of Elastin-Like Block Co-Recombinamers:The Controlled Formation of Micelles and Vesicles in an Aqueous Medium, Biomacromolecules 13 (2012) 293–298.

[28] A. Fernández-Colino, F.J. Arias, M. Alonso, J.C. Rodríguez-Cabello, Amphiphilic elastin-like block Co-recombinamers containing leucine zippers: cooperative interplay between both domains results in injectable and stable hydrogels, Biomacromolecules 16 (2015) 3389–3398.
[29] A. Fernández-Colino, F.J. Arias, M. Alonso, J.C. Rodríguez-Cabello, Self-organized ECM-Mimetic model based on an amphiphilic multiblock silk-elastin-Like corecombinamer with a concomitant dual physical gelation process, Biomacromolecules 15 (2014) 3781–3793.
[30] O. Liliang, Y. Rui, Z. Yu, S. Wei, Effect of bioink properties on printability and cell viability for 3D bioplotting of embryonic stem cells, Biofabrication 8 (2016), 035020.
[31] F. Cipriani, M. Krüger, I.G. de Torre, L.Q. Sierra, M.A. Rodrigo, L. Kock, J.C. Rodriguez-Cabello, Cartilage regeneration in preannealed silk elastin-like Co-recombinamers injectable hydrogel embedded with mature chondrocytes in an ex vivo culture platform, Biomacromolecules 19 (2018) 4333–4347.
[32] N. Paxton, W. Smolan, T. Böck, F. Melchels, J. Groll, T. Jungst, Proposal to assess printability of bioinks for extrusion-based bioprinting and evaluation of rheological properties governing bioprintability, Biofabrication 9 (2017), 044107.
[33] E. Golemis, Protein-protein Interactions: a Molecular Cloning Manual, Cold Spring Harbor Laboratory Press, Cold Spring Harbor, NY, 2002.
[34] W. Liu, M.A. Heinrich, Y. Zhou, A. Akpek, N. Hu, X. Liu, X. Guan, Z. Zhong, X. Jin, A. Khademhosseini, Y.S. Zhang, Extrusion bioprinting of shear-thinning gelatin methacryloyl bioinks, Adv. Healthc. Mater. 6 (2017), http://dx.doi.org/10.1002/adhm.201601451.
[35] J. Leppiniemi, P. Lahtinen, A. Paajanen, R. Mahlberg, S. Metsä-Kortelainen, T. Pinomaa, H. Pajari, I. Vikholm-Lundin, P. Pursula, V.P. Hytönen, 3D-printable bioactivated nanocellulose–Alginate hydrogels, ACS App. Mater.Interfaces 9 (2017) 21959–21970.
[36] J. Jia, D.J. Richards, S. Pollard, Y. Tan, J. Rodriguez, R.P. Visconti, T.C. Trusk, M.J. Yost, H. Yao, R.R. Markwald, Y. Mei, Engineering alginate as bioink for bioprinting, Acta Biomater. 10 (2014) 4323–4331.
[37] R. Lozano, L. Stevens, B.C. Thompson, K.J. Gilmore, R. Gorkin, E.M. Stewart, M. in het Panhuis, M. Romero-Ortega, G.G. Wallace, 3D printing of layered brain-like structures using peptide modified gellan gum substrates, Biomaterials 67 (2015) 264–273.
[38] C.M. Potter, K.H. Lao, L. Zeng, Q. Xu, Role of biomechanical forces in stem cell vascular lineage differentiation, Arterioscler. Thromb. Vasc. Biol. 34 (2014) 2184–2190.
[39] A. Blaeser, D.F. Duarte Campos, U. Puster, W. Richtering, M.M. Stevens, H. Fischer, Controlling shear stress in 3D bioprinting is a key factor to balance printing resolution and stem cell integrity, Adv. Healthc. Mater. 5 (2016) 326–333.
[40] S. Khetan, J.A. Burdick, Patterning network structure to spatially control cellular remodeling and stem cell fate within 3-dimensional hydrogels, Biomaterials 31 (2010) 8228–8234.
[41] A.J. Engler, S. Sen, H.L. Sweeney, D.E. Discher, Matrix elasticity directs stem cell lineage specification, Cell 126 (2006) 677–689.
[42] H. Wang, L. Cai, A. Paul, A. Enejder, S.C. Heilshorn, Hybrid Elastin-like Polypeptide–Polyethylene Glycol (ELP-PEG) Hydrogels with Improved Transparency and Independent Control of Matrix Mechanics and Cell Ligand Density, Biomacromolecules 15 (2014) 3421–3428.
[43] K.A. Kyburz, K.S. Anseth, Three-dimensional hMSC motility within peptide-functionalized PEG-based hydrogels of varying adhesivity and crosslinking density, Acta Biomater. 9 (2013) 6381–6392.
[44] A. Girotti, J. Reguera, J.C. Rodríguez-Cabello, F.J. Arias, M. Alonso, A.M. Testera, Design and bioproduction of a recombinant multi(bio)functional elastin-like protein polymer containing cell adhesion sequences for tissue engineering purposes, J. Mater. Sci. Mater. Med. 15 (2004) 479–484.
[45] B. Paiva Dos Santos, B. Garbay, M. Pasqua, E. Chevron, Z.S. Chinoy, C. Cullin, K. Bathany, S. Lecommandoux, J. Amedee, H. Oliveira, E. Garanger, Production, purification and characterization of an elastin-like polypeptide containing the Ile-Lys-Val-Ala-Val (IKVAV) peptide for tissue engineering applications, J. Biotechnol. 298 (2019) 35–44.
[46] Z. Wang, J. Guo, J. Sun, P. Liang, Y. Wei, X. Deng, W. Gao, Thermoresponsive and Protease-Cleavable Interferon-Polypeptide Conjugates with Spatiotemporally Programmed Two-Step Release Kinetics for Tumor Therapy, Adv. Sci. (Weinh) 6 (2019), 1900586-1900586.